



Article

Water-Soluble Bismuth(III) Polynuclear Tyrosinehydroximate Metallamacrocyclic Complex: Structural Parallels to Lanthanide Metallacrowns

Marina A. Katkova ^{1,*} , Grigory Y. Zhigulin ¹, Roman V. Romyantsev ¹, Galina S. Zabrodina ¹, Vladimir R. Shayapov ², Maxim N. Sokolov ^{2,3}  and Sergey Y. Ketkov ¹

¹ G.A. Razuvaev Institute of Organometallic Chemistry RAS, 603950 Nizhny Novgorod, Russia; gzhigulin@gmail.com (G.Y.Z.); romanrum@iomc.ras.ru (R.V.R.); kudgs@mail.ru (G.S.Z.); sketkov@iomc.ras.ru (S.Y.K.)

² Nikolaev Institute of Inorganic Chemistry SB RAS, 630090 Novosibirsk, Russia; vladimir@niic.nsc.ru (V.R.S.); caesar@niic.nsc.ru (M.N.S.)

³ Chemistry Department, Kazan (Volga Region) Federal University, 420097 Kazan, Russia

* Correspondence: marina@iomc.ras.ru

Academic Editor: Nikolay Gerasimchuk

Received: 27 August 2020; Accepted: 23 September 2020; Published: 23 September 2020



Abstract: Recently there has been a great deal of interest and associated research into aspects of the coordination chemistry of lanthanides and bismuth—elements that show intriguing common features. This work focuses on the synthesis and characterization of a novel bismuth(III) polynuclear metallamacrocyclic complex derived from aminohydroxamic acid, in order to compare the coordination ability of Bi³⁺ with the similarly sized La³⁺ ions. A polynuclear tyrosinehydroximate Bi(OH)[15-MC_{Cu(II)Tyra}-5](NO₃)₂ (**1**) was obtained according to the synthetic routes previously described for water-soluble Ln(III)-Cu(II) 15-MC-5 metallacrowns. Correlations between structural parameters of Bi(III) and Ln(III) complexes were analyzed. DFT calculations confirmed the similarity between molecular structures of the model bismuth(III) and lanthanum(III) tyrosinehydroximate 15-metallacrowns-5. Analysis of the electronic structures revealed, however, stronger donor-acceptor interactions between the central ion and the metallamacrocyclic in the case of the lanthanum analogue. Thermochromic properties of **1** were studied.

Keywords: bismuth(III); lanthanide(III); tyrosinehydroximate; polynuclear metallamacrocyclic complex; metallacrown; X-ray structure; DFT calculation

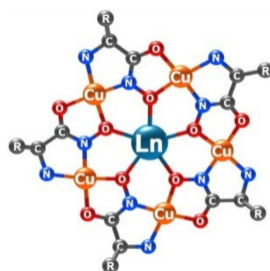
1. Introduction

Bismuth(III) complexes have received increased interest due to their high effectiveness in eradication of *Helicobacter pylori*, and also as potential antimicrobial and anti-leishmanial agents [1–3]. Up to now, many coordination bismuth(III) compounds with a large variety of ligands and coordination environments had been synthesized and explored in biomedical applications [4–8]. Recent interest in the use of alpha-emitting ²¹³Bi in nuclear medicine requires efficient Bi complexation, preferably within a macrocyclic cavity [9,10]. It is not surprising that research on the synthesis of biologically important ligands and their water-soluble complexes has received significant attention [11–17]. However, the chemistry of Bi(III) explored in this purpose to date is rather scarce, and the study of bismuth complexes in aqueous solutions is often difficult.

Bismuth is the heaviest stable element and is recognized as a relatively low toxic metal, although conversely, it sits in the Periodic table among the most toxic and radioactive elements including mercury, thallium, lead, and polonium [18]. Additionally, within group 15, antimony and arsenic compounds are generally of high toxic nature, whereas those of bismuth exhibit a significantly reduced

toxicity [19]. This behavior is probably caused by the unique electronic structure of the Bi^{3+} ion. The ground-state electron configuration of bismuth $[\text{Xe}]4f^{14}5d^{10}6s^26p^3$ is particularly stable, and the three 6p electrons are responsible for bond formation on coordination [20]. Thus, in the numerous of Bi-containing complexes, bismuth exhibits the oxidation state of 3+. Noteworthy, the Shannon ionic radii of Bi^{3+} (1.03 and 1.17 Å for coordination numbers of 6 and 8, respectively) are similar to those of La^{3+} (1.032 and 1.16 Å, respectively) [21]. Consequently, in the first approximation based on electrostatic and steric factors, analogous complexes of bismuth and the lanthanides could adopt similar coordination geometries [22]. Sometimes, however, this is not the case. Specifically, Evans et al. described the synthetic and structural results in organobismuth chemistry that allow comparisons between the coordination geometries of bismuth and the lanthanides. This study found that it is necessary to take into account that the coordination chemistry of bismuth can be influenced by a stereochemically active lone pair, and bismuth has much higher Pauling electronegativity (1.9) than that of lanthanides (1.10–1.25) [22]. These similarities and differences certainly deserve more research efforts, particularly in the exploration of novel structural motifs of more developed lanthanide chemistry in order to design and synthesize new Bi(III) compounds.

Herein, to develop the next generation of coordination Bi(III) complexes with biologically important ligands, we considered polynuclear aminohydroximate Ln(III)-Cu(II) complexes, which belong to a family of 15-MC-5 metallacrowns. The popularity of Ln(III)-Cu(II) 15-MC-5 complexes is largely due to their fascinating architectures and potential applications [23–28]. These complexes present snowflake-like structures (Scheme 1) with the neutral ring consisting of five [Cu(II)-N-O] repeating units and the five hydroximate oxygen atoms encapsulating a Ln^{3+} ion within the central cavity.



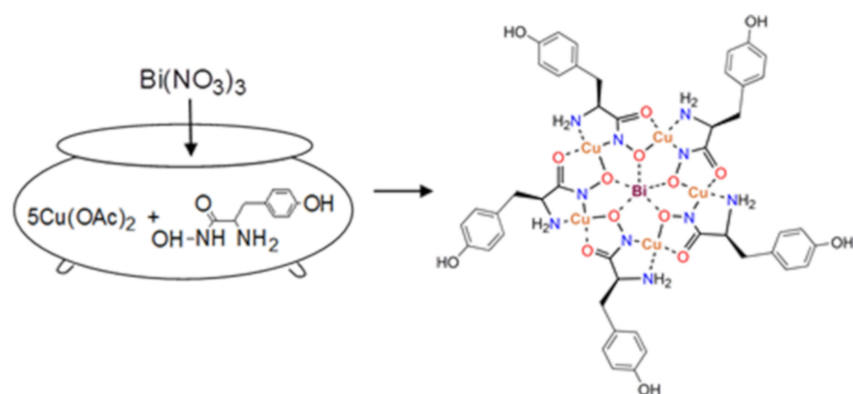
Scheme 1. Schematic representation of Ln(III)-Cu(II) [15MC-5]. Hydrogen atoms, additional anions, and solvate molecules are omitted for the sake of simplicity.

A relevant aspect of this structure is that the ligand scaffold prefers early lanthanides characterized by the same charge and similar ionic radii as Bi^{3+} . Recently, we have demonstrated the first metallamacrocyclic 15-MC-5 complex constructed from Cu^{2+} and Bi^{3+} metal centers and pyrazinohydroxamic moieties [29]. The single-crystal structure reveals the classic metallamacrocyclic 15-MC-5 configuration. The Bi^{3+} ion is located at the center of the 15-MC-5 ring consisting of five [Cu(II)-N-O] repeating units. Following our interest in water-soluble Ln(III)-Cu(II) 15-MC-5 metallacrowns with aminohydroximate ligands [30–34], we describe here a general synthetic approach and comparable characterization of a new water-soluble metallamacrocyclic Bi(III)-Cu(II) 15-MC-5 complex derived from tyrosinehydroxamic acid.

2. Results and Discussion

2.1. Synthesis and Spectroscopic Aspects

Following a previously described synthetic procedure for water-soluble Ln(III)-Cu(II) 15-MC-5 metallacrowns [30,31] we employed the most frequently used two-step methodology with some modification. In the first step, α -tyrosinehydroxamic acid and $\text{Cu}(\text{CH}_3\text{COO})_2$ were mixed in water and, in the second step, $\text{Bi}(\text{NO}_3)_3$ was added to this solution (Scheme 2).



Scheme 2. Schematic representation of the synthesis of complex **1**.

It can be seen (Figure 1) that the absorption spectra of the resulting complex **1** are similar to those of La complex. In the visible region a broad band with the maximum at 575 nm ($\epsilon = 395 \text{ M}^{-1} \text{ cm}^{-1}$), assigned to Cu(II) d-d transition, is responsible for the characteristic dark blue color, which is observed in all previously reported water-soluble Ln(III)-Cu(II) aminohydroximate complexes [23,24,30,31].

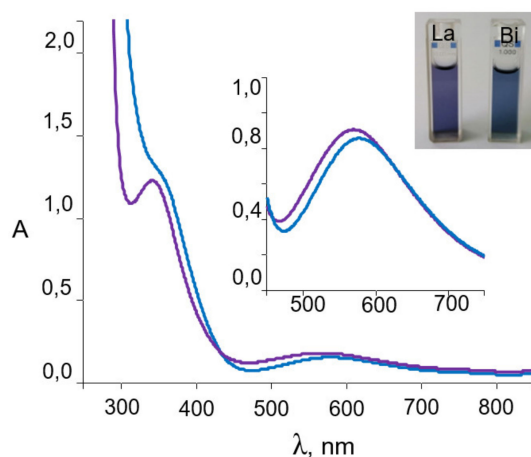


Figure 1. UV-vis spectra of the aqueous solution of **1** (blue) and the analogous La complex (violet). Inset: Spectra at 575 nm ($2.3 \times 10^{-3} \text{ M}$).

The yield of isolated crystalline **1** was 32%, in contrast to 85% of the lanthanum analogue, because of hydrolysis of Bi^{3+} in water. Crystals of **1** suitable for the single-crystal X-ray diffraction experiment were obtained by recrystallization from water. It is worth mentioning that the stability of complex **1** in aqueous solutions was confirmed using UV-vis spectroscopy by recording absorption spectra at a pH value of about 7, important for biological studies (pH 6.8). No absorbance changes even after several days were recorded in either the intensity or the position of the absorption bands. Nevertheless, in contrast to the lanthanum complexes, in alkaline medium (greater than pH 8) the rapid hydrolysis of **1** occurs with the formation of an amorphous pale precipitate.

2.2. Thermochromic Properties

Compound **1** exhibits interesting low-temperature thermochromism. Diffuse reflection spectra recorded in the range from -175 to $+21$ °C are shown in Figure 2. They show a monotonous shift toward near the IR region.

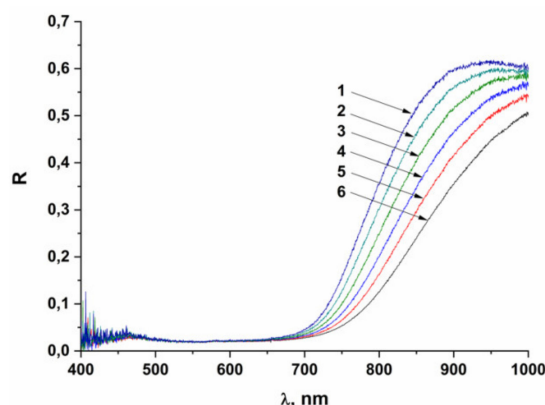


Figure 2. Diffuse reflection spectra of the sample obtained at temperatures: $-175\text{ }^{\circ}\text{C}$ (1), $-141\text{ }^{\circ}\text{C}$ (2), $-100\text{ }^{\circ}\text{C}$ (3), $-58\text{ }^{\circ}\text{C}$ (4), $-21\text{ }^{\circ}\text{C}$ (5), $+21\text{ }^{\circ}\text{C}$ (6).

To determine the absorption value from the diffuse reflection spectra, the spectra of the Kubelka-Munk function $F(R)$ were calculated:

$$F(R) = (1 - R)^2 / (2R) \quad (1)$$

where R is the diffuse reflection coefficient. The Kubelka-Munk function is directly proportional to the absorption coefficient k and inversely proportional to the scattering coefficient s of the powder, which is virtually independent on the wavelengths. Therefore, the shape of $F(R)$ qualitatively approximates the absorption spectrum. The procedure described in [35] was applied to determine the value of the gap (E_g) of interband electronic transitions. In the range of the electronic transition, the dependence of the absorption coefficient α on the energy E has the form:

$$\alpha = A(E - E_g)^m / E \quad (2)$$

where A and m are the constants of the electronic transition and E_g is its energy. In this paper we used the Kubelka-Munk function $F(R)$ as an approximation for α . This can be transformed into the following equation:

$$d \ln(\alpha E) / dE = m / (E - E_g) \quad (3)$$

which provides a simple way to determine E_g , since the value of E_g will correspond to the maximum of this function. As an example, the dependence obtained at $-175\text{ }^{\circ}\text{C}$ is given in Figure 3.

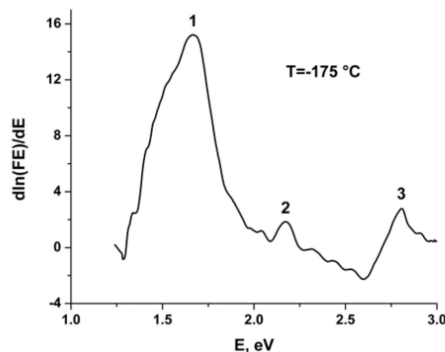


Figure 3. Dependence of $d \ln(F(R) \cdot E) / dE$ on energy at $-175\text{ }^{\circ}\text{C}$.

The 1–3 maxima (Figure 3) can be assigned to the $d_z^2 \rightarrow d_{x^2-y^2}$ (742 nm), $d_{xy} \rightarrow d_{x^2-y^2}$ (571 nm), and $d_{xz,yz} \rightarrow d_{x^2-y^2}$ (446 nm) transitions, respectively. These d-d transitions are expected for the Cu^{2+}

ion in square planar and square pyramidal coordination environment. The first transition formally corresponds to the band gap and is temperature-dependent (Figure 4).

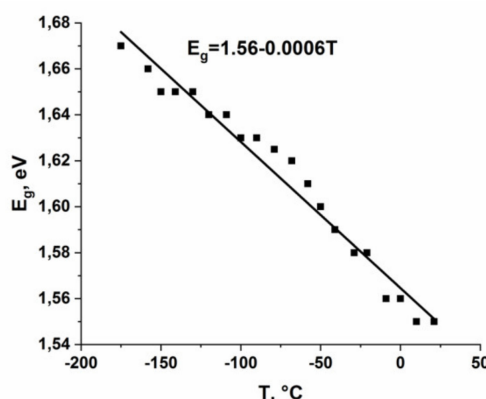


Figure 4. Temperature dependence of the $d_z^2 \rightarrow d_{x^2-y^2}$ transition energy (points) and its linear approximation (solid line). The graph shows the equation of a straight line that describes the experimental points in the best possible way.

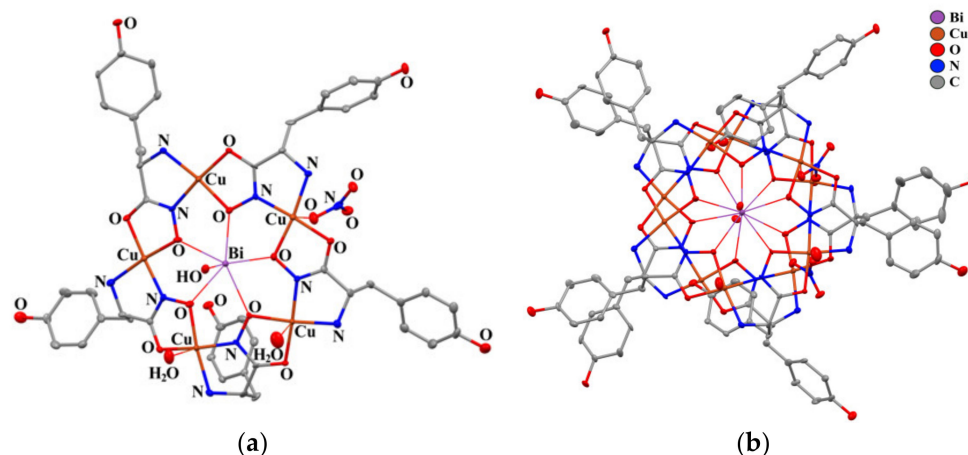
Such a behavior might reflect a decrease of the bond lengths under cooling [36], which increases the antibonding $d_{x^2-y^2}$ orbital energy and the width of the band gap (the HOMO-LUMO gap in an isolated complex). The temperature dependence of the other d-d transitions is very weak. This can be caused by the π -admixture to the corresponding occupied d orbitals (they are π^* -antibonding), which also results in an increase of their energies on cooling and reduces the band gap, therefore off-setting the influence of the raising $d_{x^2-y^2}$ energy on the electronic transitions.

2.3. Structural Aspects: X-Ray Crystal Structure

The X-ray crystal structure of **1** (Table 1) reveals the classic metallamacrocyclic 15-MC-5 configuration. The structure of **1** is depicted in Figure 5. The structural unit consists of two independent monomeric molecules (A and B) of the metallamacrocyclic Bi(III)–Cu(II) tyrosinehydroximate complex (Figure 5a). The molecules A and B have similar structures. The Bi atom is located at the center of the 15-MC_{Cu(II)Tyrlha}-5 ring, and is coordinated by five oxygen atoms of the ring in the equatorial plane. This Bi³⁺ complex **1** is expected to be isostructural to its La³⁺ analogue, since the ionic radii of both ions are comparable. However, according to the Cambridge Crystallographic Data Centre, no X-ray structural data on the La(III)–Cu(II) tyrosinehydroximate complexes have been reported thus far. Since the difference in the ionic radii between Bi³⁺ (CN = 6) and Gd³⁺ (CN = 8) is only 0.023 Å [21], the geometric characteristics of molecules **1** and known Gd(III)–Cu(II) tyrosinehydroximate complex are expectedly similar (Table 1), and the geometry of the Gd³⁺ complex can be used as reference. The crystallographic parameters of the gadolinium complex ($a = 15.02060(10)$ Å, $b = 28.9110(2)$ Å, $c = 16.42480(10)$ Å, $\beta = 103.9510(10)^\circ$, $V = 6922.24(8)$ Å³, space group I2) [37] are also close to the corresponding values of crystal **1** ($a = 14.7255(6)$ Å, $b = 28.8331(12)$ Å, $c = 16.2230(7)$ Å, $\beta = 104.3559(16)^\circ$, $V = 6672.9(5)$ Å³, space group P2(1)).

Table 1. Comparison of X-ray structural parameters of complex **1** with Bi(Cl)(H₂O)[15-MC_{Cu(II)}Pyzha-5](NO₃)₂ [29] and Gd(H₂O)₃[15-MC_{Cu(II)}Tyrha-5](NO₃)₃ complexes [37].

Distances [Å] and angles [°]	1A (M = Bi)	1B (M = Bi)	Bi(Cl)(H ₂ O)[15-MC _{Cu(II)} Pyzha-5] [29]	Gd(H ₂ O) ₃ [15-MC _{Cu(II)} Tyrha-5] [37]
M-O(oxime)	2.387(7)–2.506(8)	2.412(8)–2.543(8)	2.429(8)–2.451(7)	2.406(5)–2.440(7)
Cu-O(oxime)	1.911(7)–1.935(8)	1.915(8)–1.941(9)	1.912(8)–1.928(7)	1.908(5)–1.944(6)
Cu-O(carbonyl)	1.905(8)–1.961(8)	1.916(8)–1.952(8)	1.935(7)–1.951(7)	1.909(7)–1.959(9)
Cu-N(imine)	1.903(9)–1.914(10)	1.898(10)–1.912(10)	1.906(8)–1.947(10)	1.866(9)–1.904(6)
Cu-N(amine)	1.990(9)–2.021(9)	2.000(9)–2.027(10)	2.006(9)–2.024(10)	1.990(9)–2.037(9)
Cu-O(solv)	2.48(1), 2.57(2)	2.42(1), 2.56(1)	2.16(2)–2.37(1)	2.553(9)
M-O(OH/H ₂ O)	2.106(8)	2.047(7)	2.555(10)	2.35(1)–2.54(2)
Cu-O(NO ₃)	2.44(1), 2.88(1)	2.425(8), 2.95(1)	2.32(2)–2.403(8)	2.477(7), 2.95(1)
Cu-O(Tyrha)	2.762(8)	2.655(8)	-	2.825(7)
M...M (across the dimer cavity)	7.1742(6)	-	-	8.3933(6)
M...M (between dimers)	9.2437(8)	-	-	8.5158(6)
O(oxime)-Cu-N(imine)	90.8(4)–91.0(4)	90.6(4)–91.5(4)	89.5(3)–90.9(4)	89.3(3)–90.9(4)
O(oxime)-M-O(oxime)	70.6(3)–73.8(3)	71.0(3)–72.9(3)	71.5(3)–72.9(3)	70.7(2)–71.5(2)

**Figure 5.** Top views of the structure of complex **1**: (a) monomer and (b) dimer pair shown looking down the pseudo fivefold axis. The thermal ellipsoids drawn are at the 30% probability level. All hydrogen atoms, uncoordinated NO₃[−] and solvate water molecules are omitted for clarity.

Note that the gadolinium atom in complex Gd(H₂O)₃[15-MC_{Cu(II)}Tyrha-5](NO₃)₃ [37] is additionally coordinated by three oxygen atoms of water molecules (two of which are located on one side in respect to Cu₅ plane while the third on the other). In contrast to the lanthanide analogues, the Bi³⁺ ion is additionally coordinated by only one oxygen atom of the hydroxide anion in an apical position. The Bi-O distance (2.047(7), 2.106(8) Å) is in excellent agreement with the literature data on the compounds with the Bi-OH bonds [38–40]. The nearest water molecules are at the distance of 2.920(8) and 2.996(8) Å from Bi in the A and B molecules, respectively. These values significantly exceed the sum of the ionic radius of Bi³⁺ (1.03 Å) [21] and the van der Waals radius of the oxygen atom (1.55 Å) [41]. Thus, the coordination number of the bismuth atoms in both molecules is six, and the coordination environment is a pentagonal pyramid.

Two copper atoms additionally coordinate the water molecule in each of the independent molecules. One copper atom in each of the independent molecules has a strong interaction with the nitrate anion. Two NO₃[−] anions in the independent part of the cell are not coordinated to the metal atoms or the interaction is very weak. The closest distances of the oxygen atoms of these anions to the copper atoms are 2.924, 3.101, 3.157, and 3.267 Å.

The planes of the metallacrown rings are largely distorted. The average deviations of atoms from the plane are 0.18 and 0.16 Å for molecules A and B, respectively. It should be noted that the central

bismuth atoms are localized practically in the plane of the metallacrown rings. The deviation of the Bi^{3+} ions from these planes are 0.036(A) and 0.184(B) Å.

A comparison of the related complex of bismuth with pyrazinohydroxamic acid [29] reveals significant differences in the crystal packing between these two compounds. The molecules of the bismuth complex with pyrazinohydroximate ligands form an infinite three-dimensional (3D) network due to $\text{N}\cdots\text{H}$ interactions and $\pi\cdots\pi$ stacking. Neighboring molecules are largely offset from each other and do not form dimeric motifs. In contrast, in complex **1**, one copper atom of the metallacrown ring is additionally coordinated by the hydroxyl oxygen atom of a neighboring molecule. The $\text{Cu-O}(\text{Tyrha})$ distances are 2.762(8) and 2.655(8) Å. Due to these interactions, the molecules of complex **1** form dimeric associates in the crystal (Figure 6). In addition, the coordinated NO_3^- anions are arranged in such a way that one of the oxygen atoms is oriented toward the copper atom of the partner molecule in the dimeric species. The intermolecular distances of $\text{Cu-O}(\text{NO}_3^-)$ are 2.88 (1) and 2.95 (1) Å.

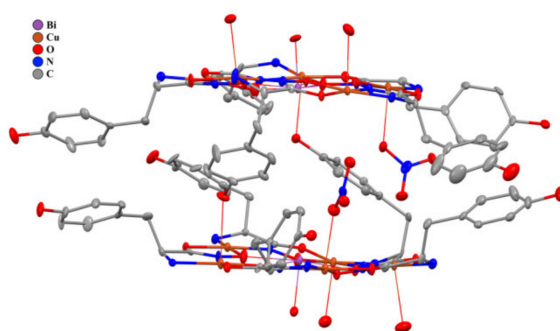


Figure 6. Side view of molecular structure of complex **1**. The thermal ellipsoids drawn are at the 30% probability level. All hydrogen atoms, uncoordinated NO_3^- , and solvate water molecules are omitted for clarity.

Note that the crystal packing of complex **1** (Figure 7) is similar to that found in the gadolinium (III) tyrosinehydroximate complex [37]. Three water molecules are located inside the dimer cavity, both in complex **1** and in the gadolinium tyrosinehydroximate complex [37]. However, in the case of gadolinium, two water molecules are coordinated to Gd^{3+} . Thus, the Gd-O bonds are almost perpendicular to the planes of the metallacrown rings. In turn, in complex **1**, the water molecules are significantly displaced from such an ideal position. This leads to the $\text{Bi}\cdots\text{Bi}$ distance in the dimers in **1** (7.17 Å) being much shorter than the corresponding $\text{Gd}\cdots\text{Gd}$ distance (8.39 Å). The distances between the copper atom and the hydroxyl group of tyrosinehydroximate ligand of the neighboring metallacrown are also significantly shorter in complex **1** (Table 1). In turn, the distance between dimer particles is shorter in the gadolinium complex ($d(\text{Gd} \dots \text{Gd}) = 8.52$ Å) [37] than the $\text{Bi}\cdots\text{Bi}$ distances in complex **1** (9.24 Å).

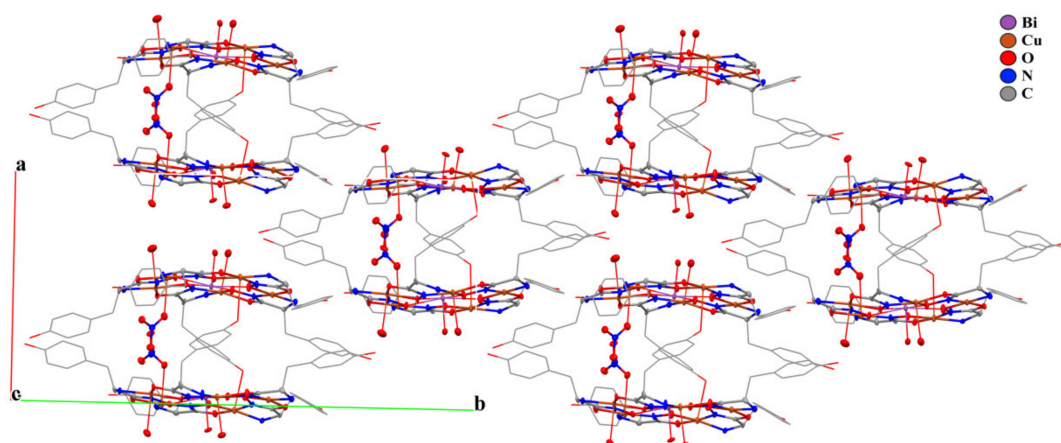


Figure 7. Fragment of crystal packing of complex **1**. All hydrogen atoms, uncoordinated NO_3^- , and solvate water molecules are omitted for clarity.

2.4. Theoretical Calculations

To shed some light on the exceptional bonding of **1**, DFT calculations were performed in this work. In contrast to the Bi complex bearing one OH^- group, the La 15-MC-5 complexes contain typically 4 H_2O molecules coordinated at the axial positions of the La^{3+} ion. To provide comparable results when studying the bismuth(III) and lanthanum(III) ion influence on the metallamacrocyclic environment in the tyrosinehydroximate 15-metallacrowns-5, we analyzed the Bi and La model complexes without axial OH^- and H_2O ligands $[\text{M}(15\text{-MC}_{\text{Cu(II)Tyrha-5}})]^{3+}$ ($\text{M} = \text{Bi, La}$). Both structures were optimized at the scalar relativistic SR-PBE/rL2 level of DFT with the XRD atomic coordinates of complex **1** being used as the initial geometry approximation. Optimized interatomic distances of the $[\text{Bi}(15\text{-MC}_{\text{Cu(II)Tyrha-5}})]^{3+}$ complex agree well with the experimental values of **1** (Tables 1–3). Moreover, the optimized structure of $[\text{La}(15\text{-MC}_{\text{Cu(II)Tyrha-5}})]^{3+}$ appeared to be very similar to that of the bismuth derivative. The topological analysis of the electron density function $\rho(\mathbf{r}_c)$ reveals negative values of the Laplacian $\nabla^2\rho(\mathbf{r}_c)$ for covalent bonds at the (3,-1) critical points (Table 2) and positive $\nabla^2\rho(\mathbf{r}_c)$ values for the Cu-N, Cu-O, Bi-O, and La-O coordination bonds (Table 3). In the tyrosinehydroximate ligands, adjacent C- N_{im} and C-O bonds are characterized by higher values of the electron density $\rho(\mathbf{r}_c)$ and ellipticity ϵ at the (3,-1) critical points (0.358–0.362 a.u. and 0.099–0.289, respectively, Table 2). This indicates a π -delocalization among the N_{im} , C, and O_{carb} atoms in the hydroximate chelates with the π -contributions into the C- N_{im} bonds being higher ($\epsilon = 0.277$ – 0.289) than those for C-O ($\epsilon = 0.099$ – 0.107). Ellipticity values of 0.175–0.195 calculated for the aromatic C-C bonds in the $\text{C}_6\text{H}_4\text{OH}$ fragments are intermediate between those for C- N_{im} and C-O. Ellipticity values of 0.059–0.070 obtained for the N-O single bonds suggest some p,π -conjugation between the oxime oxygen lone pair and the delocalized π -system. Additionally, p,π -conjugation is expected to occur for C-O(H) bonds in the substituents ($\epsilon = 0.077$ – 0.078). The C-C bonds in the hydroximate chelates (1.517–1.523 Å) are shorter than typical single C-C bonds (1.54 Å). Taking into account calculated ellipticity values of 0.104–0.107 one can assume the σ,π -conjugation (hyperconjugation) effect. Such interaction is also inherent in the single C- C_{ring} bonds (1.508–1.510 Å) between the H_2C and $\text{C}_6\text{H}_4\text{OH}$ fragments of the substituents ($\epsilon = 0.043$ – 0.049). For comparison: C- C_{R} bonds between the hydroximate chelates and the substituents without σ,π -conjugation are characterized by the 1.547–1.552 Å lengths and ellipticity values close to zero (0.018–0.021).

Table 2. Optimized interatomic distances and topological parameters at the (3,-1) critical points of the covalent bonds in the $[\text{Bi}(15\text{-MC}_{\text{Cu(II)Tyrha-5}})]^{3+}/[\text{La}(15\text{-MC}_{\text{Cu(II)Tyrha-5}})]^{3+}$ complexes. The level of DFT calculations is SR-PBE/rL2.

Atoms	Distance, Å	$\rho(\mathbf{r}_c)$, a.u.	$\nabla^2\rho(\mathbf{r}_c)$, a.u.	ϵ
C-C ¹	1.517–1.523/	0.250–0.252/	–(0.508–0.494)/	0.106–0.107/
	1.518–1.523	0.249–0.252	–0.014	0.104–0.105
C-N _{am} ²	1.494–1.498/	0.244–0.246/	–(0.485–0.475)/	0.016–0.019/
	1.495–1.500	0.244–0.246	–0.011	0.016–0.018
C-N _{im} ²	1.323/	0.358–0.359/	–(1.177–1.172)/	0.277–0.279/
	1.317–1.318	0.362	–0.006	0.287–0.289
C-O	1.283–1.284/	0.361–0.362/	–(0.862–0.850)/	0.104–0.107/
	1.285–1.286	0.36	–0.011	0.099–0.102
N-O	1.381–1.382/	0.323–0.324/	–(0.131–0.128)/	0.069–0.070/
	1.395–1.396	0.311–0.312	–0.003	0.059–0.060
C-C _R ³	1.549–1.552/	0.227–0.228/	–(0.380–0.375)/	0.018–0.021/
	1.547–1.550	0.228–0.230	–0.008	0.018–0.021
C-C _{ring} ⁴	1.508–1.509/	0.248/	–(0.495–0.494)/	0.044–0.049/
	1.508–1.510	0.247–0.248	–0.003	0.043–0.048

¹ C-C is the bond between the carbon atoms of the hydroximate chelate. ² Herein after indices “am” and “im” correspond to the amine and imine nitrogen atoms respectively. ³ C-C_R is the bond between the hydroximate chelate and the R = CH₂(C₆H₄)OH substituent. ⁴ C-C_{ring} is the bond between the CH₂ and (C₆H₄)OH fragments.

Table 3. Optimized interatomic distances, topological, and energy parameters at the (3,-1) critical points of the coordination bonds in the $[\text{Bi}(15\text{-MC}_{\text{Cu(II)Tyrha-5}})]^{3+}/[\text{La}(15\text{-MC}_{\text{Cu(II)Tyrha-5}})]^{3+}$ complexes. Table 2.

Atoms	Distance, Å	$\rho(\mathbf{r}_c)$, a.u.	$\nabla^2\rho(\mathbf{r}_c)$, a.u.	$V(\mathbf{r}_c)$, a.u.	E_{int} , kcal/mol	ϵ
Bi-O _{ox} ^{1/}	2.433–2.442/	0.049–0.050/	0.167–0.170/	–(0.053–0.052)/	16.3–16.8/	0.182–0.184/
La-O _{ox} ¹	2.432–2.438	0.056–0.057	0.187–0.189	–0.001	19.8–20.2	0.240–0.241
Cu-O _{ox} ¹	1.973–1.984/	0.084–0.086/	0.381–0.396/	–(0.129–0.124)/	38.8–40.4/	0.047–0.048/
	1.992–2.006	0.080–0.082	0.352–0.369	–0.006	35.9–37.7	0.041–0.042
Cu-O _{carb} ¹	1.933–1.936/	0.094/	0.444–0.447/	–(0.150–0.148)/	46.5–47.0/	0.014–0.018/
	1.934–1.937	0.094	0.442–0.446	–0.001	46.3–46.9	0.023–0.027
Cu-N _{im}	1.890–1.892/	0.114–0.115/	0.474–0.477/	–(0.195–0.194)/	60.9–61.3/	0.071–0.074/
	1.896–1.897	0.113	0.464–0.468	–0.191	59.9–60.1	0.071–0.074
Cu-N _{am}	2.034–2.049/	0.083–0.086/	0.281–0.293/	–(0.121–0.115)/	36.0–37.9/	0.020–0.023/
	2.036–2.054	0.083–0.086	0.277–0.292	–0.007	35.4–37.6	0.019–0.021

¹ Herein after indices “ox” and “carb” correspond to the oxime and carbonyl oxygen atoms, respectively.

Among the copper(II) coordination bonds the interactions with the imine nitrogen atoms of the tyrosinehydroximate ligands are estimated as the strongest ones with calculated energies of 59.9–61.3 kcal/mol (Table 3). The more elongated contacts with the amine nitrogen atoms are characterized by the lower values of 35.4–37.9 kcal/mol. Energies of copper(II) bonds with the oxime and carbonyl oxygen atoms are closer: 35.9–40.4 and 46.3–47.0 kcal/mol, respectively. In general, the bonding situation in the hydroximate chelates of the $[\text{M}(15\text{-MC}_{\text{Cu(II)Tyrha-5}})]^{3+}$ complexes is similar to that in the 15-metallacrowns-5 analyzed by us earlier with use of QTAIM in conjunction with the hybrid functionals $\tau\text{-HCTHhyb}$ [33] and M06 [29,42,43]. This makes the SR-PBE/rL2 calculations appropriate for description of the hydroximate 15-metallacrowns-5.

Calculated M-O_{ox} distances are very close: 2.433–2.442 Å in $[\text{Bi}(15\text{-MC}_{\text{Cu(II)Tyrha-5}})]^{3+}$ and 2.432–2.438 Å in $[\text{La}(15\text{-MC}_{\text{Cu(II)Tyrha-5}})]^{3+}$. These coordination bonds are characterized by the lower values of $\rho(\mathbf{r}_c)$ and E_{int} (0.049–0.057 a.u. and 16.3–20.2 kcal/mol respectively, Table 3) as compared with Cu(II)-O ($\rho(\mathbf{r}_c) = 0.080\text{--}0.094$ a.u., $E_{\text{int}} = 35.9\text{--}47.0$ kcal/mol). Despite the small difference in the bond lengths the topological analysis reveals increase of the electron density at the (3,-1) critical points

on going from Bi-O_{ox} (0.049–0.050 a.u.) to La-O_{ox} (0.056–0.057 a.u.) contacts. This is accompanied by increase of the interaction energies from 16.3–16.8 kcal/mol to 19.8–20.2 kcal/mol (or from 82.8 to 99.9 kcal/mol in total). Moreover, some decrease of the electron density occurs at the (3,–1) critical points of the adjacent Cu-O_{ox} and N-O bonds. In the [Bi(15-MC_{Cu(II)Tyrha}-5)]³⁺ complex the calculated $\rho(\mathbf{r}_c)$ values are 0.084–0.086 and 0.323–0.324 a.u. for Cu-O_{ox} and N-O bonds, respectively. In the [La(15-MC_{Cu(II)Tyrha}-5)]³⁺ complex $\rho(\mathbf{r}_c) = 0.080$ –0.082 a.u. for Cu-O_{ox} and 0.311–0.312 a.u. for N-O. Accordingly, energies of the Cu-O_{ox} interactions decrease slightly from 38.8–40.4 to 35.9–37.7 kcal/mol. In addition, one principal difference between the Cu(II)-O and M-O_{ox} interactions revealed by the topological analysis is a drastic inequality of the ellipticities. Corresponding values for M-O_{ox} contacts are significantly higher (0.182–0.241) than those for copper(II) bonds (0.014–0.074). Thus, a special role in the bonding between the oxime oxygen atoms and the central ion is played by the π -interactions. At the (3,–1) critical points of the La-O_{ox} bonds the π -contributions appeared to be higher than those for the Bi-O_{ox} contacts ($\epsilon = 0.240$ –0.241 and 0.182–0.184, respectively).

In the plane of the oxime oxygen atoms O(1), O(2), and O(3) distribution of the Deformation Electron Density (DED) investigated at the PBE/x2c-TZVPall//SR-PBE/rL2 level reveals some stretch of the lone pairs toward the La³⁺ ion unlike Bi³⁺ (Figure 8). The flattened shape of the oxygen lone pairs in [Bi(15-MC_{Cu(II)Tyrha}-5)]³⁺ appears to be associated with higher σ -contribution into the Bi-O_{ox} interactions. Meanwhile, the larger density accumulation at the axial positions of the Bi³⁺ ion as compared with La³⁺ is clearly demonstrated by the DED isosurface together with the π -interactions (Figure 9). This results in the less effective positive charge on the central Bi ion and the less negative charges on the oxime oxygen atoms. The Mulliken charges calculated at the PBE/x2c-TZVPall//SR-PBE/rL2 level are +1.022*e* on Bi and –(0.436–0.434)*e* on the oxime oxygen atoms in [Bi(15-MC_{Cu(II)Tyrha}-5)]³⁺; +1.601*e* on La and –(0.533–0.530)*e* on the oxime oxygen atoms in [La(15-MC_{Cu(II)Tyrha}-5)]³⁺. The Mulliken charges calculated at the SR-PBE/rL2 level are +1.008*e* on Bi and –(0.398–0.397)*e* on the oxime oxygen atoms in [Bi(15-MC_{Cu(II)Tyrha}-5)]³⁺; +1.592*e* on La and –(0.439–0.437)*e* on the oxime oxygen atoms in [La(15-MC_{Cu(II)Tyrha}-5)]³⁺. The increase in the positive charge of the central ion on going from [Bi(15-MC_{Cu(II)Tyrha}-5)]³⁺ to [La(15-MC_{Cu(II)Tyrha}-5)]³⁺ is also predicted by the Bader QT AIM approach at the PBE/x2c-TZVPall//SR-PBE/rL2 level (+1.911*e* on Bi and +2.041*e* on La). On the basis of our calculations, one can conclude that accumulation of the density at the axial positions of the Bi³⁺ ion together with its decreased positive charge prevents filling the Bi³⁺ coordination sphere by the solvent molecules. This leads to the more effective bonding with the HO[–] negative ion in **1** (as well with Cl[–] in the pyrazinohydroximate complex [29]). As a result, the Bi³⁺ ion in the complex is characterized by the lower coordination number as compared with the La(III) 15-metallacrowns-5 where the La³⁺ central ion bears four H₂O molecules at the axial positions [33]. Accordingly, the higher DED accumulation in the axial positions of the Bi³⁺ ion induces weakening of the Bi-O_{ox} donor-acceptor interactions in comparison with the La-O_{ox} contacts that has been described above.

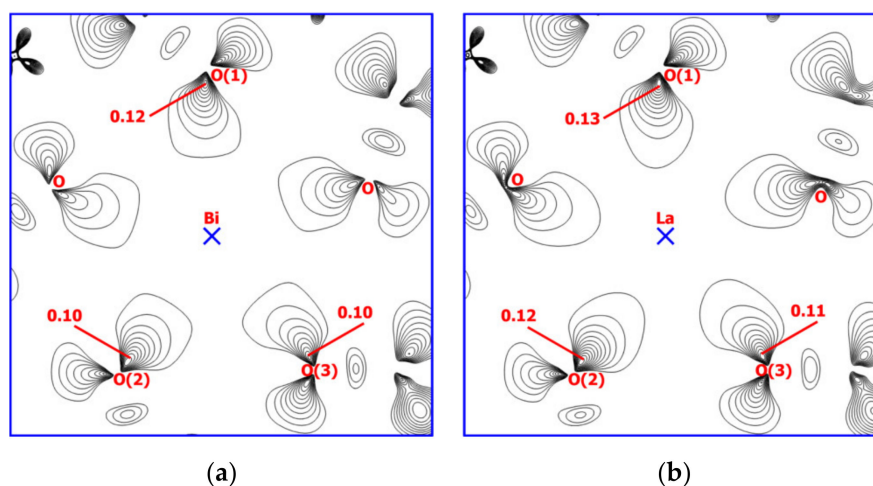


Figure 8. Deformation Electron Density maps in the plane of the oxime atoms O(1), O(2), and O(3): (a) For $[\text{Bi}(15\text{-MC}_{\text{Cu(II)Tyrha-5}})]^{3+}$; (b) For $[\text{La}(15\text{-MC}_{\text{Cu(II)Tyrha-5}})]^{3+}$. The contour lines start from 0.01 a.u. with step of 0.01 a.u. The maps are built at the same scale. The level of DFT calculations is PBE/x2c-TZVPall//SR-PBE/rL2.

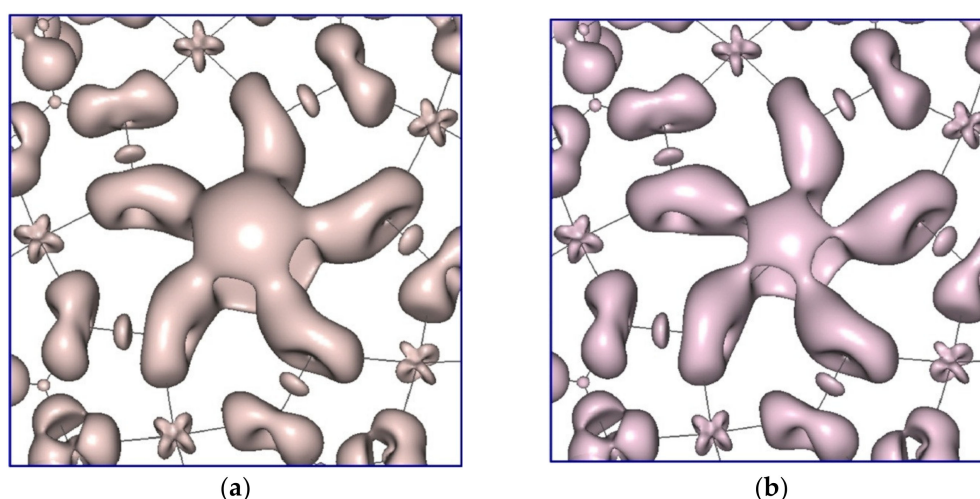


Figure 9. Deformation Electron Density isosurfaces at 0.01 a.u. in the region of the central ion and the five oxime oxygen atoms: (a) for $[\text{Bi}(15\text{-MC}_{\text{Cu(II)Tyrha-5}})]^{3+}$; (b) for $[\text{La}(15\text{-MC}_{\text{Cu(II)Tyrha-5}})]^{3+}$. The isosurfaces are built at the same scale. The level of DFT calculations is PBE/x2c-TZVPall//SR-PBE/rL2.

3. Materials and Methods

All chemicals were reagent-grade and were used as received from Sigma Aldrich without further purification. The C, H, and N elemental analyses were performed by the Microanalytical laboratory of IOMC on Euro EA 3000 Elemental Analyzer. Electronic absorption spectra were recorded with the Perkin Elmer Lambda 25 UV/Vis spectrophotometer at room temperature, at 200–1100 nm. IR spectra were obtained on a Perkin Elmer 577 spectrometer and recorded from 4000 to 450 cm^{-1} as a Nujol mull on KBr plates. ^1H NMR spectra were recorded on BrukerAvance III 400 MHz spectrometer. Samples were dissolved in high purity D_2O (Sigma Aldrich, St Louis, MO, USA), and the chemical shifts were referenced to the solvent peak. Diffuse reflection spectra were measured with a spectrophotometric system consisting of a Kolibri-2 spectrometer (VMK “Optoelectronika,” Novosibirsk, Russia), an FCR-7UV400-2-ME reflection/backscattering probe (Avantes, The Netherlands), and an AvaLight-DHS light source (Avantes, The Netherlands) [35]. The spectra were recorded in the 400–1000 nm range. BaSO_4 powder was used as a reference for 100% reflection. Temperature

measurements of the reflection spectra were performed from $-175\text{ }^{\circ}\text{C}$ to room temperature at 20 temperature points.

3.1. Synthesis

$\text{Bi}(\text{OH})[15\text{-MC}_{\text{Cu}(\text{II})\text{Tyrha-5}}](\text{NO}_3)_2$ (**1**). $\text{Bi}(\text{NO}_3)_3 \cdot 5\text{H}_2\text{O}$ (0.097 g, 0.2 mmol) was added to a stirred solution of L-tyrosinehydroxamic acid (0.196 g, 1 mmol) and $\text{Cu}(\text{OAc})_2 \cdot \text{H}_2\text{O}$ (0.199 g, 1 mmol) in 50 mL of water. After stirring overnight and filtering, the solution was left to evaporate slowly. After two days dark-blue precipitate was formed and then filtered. The crystals were dissolved in hot water and recrystallized. Yield: 0.12 g (32%). Anal. calcd for $\text{C}_{90}\text{H}_{154}\text{Cu}_{10}\text{Bi}_2\text{N}_{24}\text{O}_{70}$ (3745.72): C 28.86, H 4.14, N 8.97. Found: C 28.92, H 4.11, N 8.95. IR (ν , cm^{-1}): 3238 w, 1581 s, 1515 s, 1402 w, 1327 m, 1239 m, 1175 m, 1128 w, 1104 m, 1073 m, 1026 s, 965 w, 938 m, 852 w, 825 w, 808 s, 739 w, 648 w, 629 w, 598 m, 568 w, 543 w, 496 m. ^1H NMR (D_2O , 400 MHz, 298 K, δ_{ppm}): 7.65 (br.s, 2H, C_6H_4); 7.88 (s, 2H, CH_2); 8.9–9.5 (m, 2H, C_6H_4); 54.3 (s, 1H, CH).

3.2. X-ray Crystallographic Studies

The X-ray diffraction data for **1** were collected on Bruker D8 Quest diffractometer (graphite-monochromator, $\text{MoK}\alpha$ -radiation, ω -scan technique, $\lambda = 0.71073\text{ \AA}$, $T = 100(2)\text{ K}$). The intensity data were integrated by using the SAINT program [44]. The SADABS program [45] was used to perform area-detector scaling and absorption corrections. The structure was solved by dual method [46] and was refined on F^2 using all reflections with the SHELXTL package [47]. All non-hydrogen atoms were refined anisotropically. Hydrogen atoms were placed in calculated positions and refined in the riding-model ($U_{\text{iso}}(\text{H}) = 1.5U_{\text{eq}}(\text{O})$ in OH-groups and $U_{\text{iso}}(\text{H}) = 1.2U_{\text{eq}}(\text{C}, \text{N})$ in other groups). There are 22.7 water molecules in the unit cell per molecule of the complex. For all water molecules and hydroxide anions in **1**, the hydrogen atoms were not located.

The crystal data for **1** ($\text{C}_{90}\text{H}_{154}\text{Bi}_2\text{Cu}_{10}\text{N}_{24}\text{O}_{70}$): monoclinic crystal system, space group $\text{P}2_1$, unit cell dimensions: $a = 14.7255(6)\text{ \AA}$, $b = 28.8331(12)\text{ \AA}$, $c = 16.2230(7)\text{ \AA}$, $\beta = 104.3559(16)^{\circ}$, $V = 6672.9(5)\text{ \AA}^3$, $Z = 2$, $d_{\text{calc.}} = 1.864\text{ gcm}^{-3}$, $\mu = 4.294\text{ mm}^{-1}$, $F(000) = 3756$, Crystal size $0.21 \times 0.10 \times 0.06\text{ mm}^3$, $1.917 < \theta < 24.999$, reflections collected/unique = 68837/23130, $R_{\text{int}} = 0.0504$, $R_1 = 0.0448$, $wR^2 = 0.0938$ ($I > 2s(I)$), $R_1 = 0.0572$, $wR^2 = 0.0972$ (all data), $S(F^2) = 1.042$, largest diff. peak and hole 3.034 and $-1.495\text{ e}\text{\AA}^{-3}$. CCDC 2009753 for **1** contains the supplementary crystallographic data for this paper. These data can also be obtained free of charge at www.ccdc.cam.ac.uk/structures from the Cambridge Crystallographic Data Centre.

3.3. Computational Methodology

Our quantum chemical investigations of the $[\text{M}(15\text{-MC}_{\text{Cu}(\text{II})\text{Tyrha-5}})]^{3+}$ complexes ($\text{M} = \text{Bi}, \text{La}$) are based on the Density Functional Theory (DFT), the topological analysis of the electron density function, and studies of the Deformation Electron Density (DED) distribution. Full geometry optimizations of the complexes were performed with the Priroda 15 [48,49] software employing the PBE functional [50] in conjunction with the four-component one-electron scalar relativistic (SR) approximation to the full Dirac equation where all spin-orbit terms are neglected. For all atoms we used the original all-electron relativistic correlation-consistent rL2 basis set of the triple- ζ polarized quality [51], which is an analogue of the well-known cc-pVTZ. The complexes were treated as high-spin sextet systems without symmetry constraints. For the SCF convergence criterion, a value of 10^{-6} was assigned. Tolerance on the gradient achieved in the geometry optimizations is 10^{-5} . For accuracy of the integration grid, a value of 10^{-8} per atom was used. Harmonic vibrational frequencies were calculated to ensure the optimized stationary points to be local minima without negative eigenvalues. Assignment of the “print=+density” keyword in the Priroda 15 code allowed us to obtain values of the electron density $\rho(\mathbf{r}_c)$ at the critical points and

corresponding eigenvalues λ_1 , λ_2 , and λ_3 of the hessian $\mathbf{A}(\mathbf{r}_c)$. Thus, Laplacian $\nabla^2 \rho(\mathbf{r}_c)$ and ellipticity ε values at the critical points were calculated with the Equations (4) and (5) [52]:

$$\nabla^2 \rho(\mathbf{r}_c) = \lambda_1 + \lambda_2 + \lambda_3 \quad (4)$$

$$\varepsilon = \lambda_1 / \lambda_2 - 1 \quad (5)$$

One of the important applications of the topological analysis is the estimation of interatomic interaction energies (E_{int}) on the basis of the Espinosa correlation [53]. Initially, Equation (6) was proposed for hydrogen bond energy calculations. Later, its usage was extended to coordination bonds in metal complexes [54,55]. We calculated values of the potential electron energy density $V(\mathbf{r}_c)$ at the critical points with the Equation (7) based on the approximation of the kinetic electron energy density [56] and the virial theorem [52]:

$$E_{\text{int}} = -(1/2)V(\mathbf{r}_c) \quad (6)$$

$$V(\mathbf{r}_c) = -(3/5)(3\pi^2)^{2/3} \rho(\mathbf{r}_c)^{5/3} - (1/12)\nabla^2 \rho(\mathbf{r}_c) \quad (7)$$

Calculations of atomic charges by the Bader approach [52] were performed employing the Sculpt basin integration algorithm implemented in the AIMAll software [57]. The DED maps and isosurfaces were obtained with the Multiwfn code [58,59] using the wave functions computed with the Gaussian 09 package [60]. Corresponding Single Point Energy calculations were carried out for the molecular geometries optimized before with the Priroda 15 software. The PBE functional and the all-electron triple- ζ polarized x2c-TZVPall basis set [61] were applied at the Gaussian 09 calculations. Additionally, the ultrafine integration grid and default SCF convergence criteria without symmetry constraints were assigned (“Int = UltraFine” and “NoSymm” keywords in the Gaussian 09 code). The wave functions of the complexes were proven to be stable by the tests for the SCF solutions stability.

4. Conclusions

The identical charge and ionic radii of Bi^{3+} and La^{3+} cations open up the possibility for the development of Bi(III)-based metallacrowns. Based on this analogy, we have designed and isolated a novel example of Bi(III)-Cu(II) hydroximate metallamacrocyclic complex of the 15-MC-5 type. The single crystal X-ray diffraction measurements confirmed the classic metallamacrocyclic 15-MC-5 configuration with the neutral ring consisting of five [Cu(II)-N-O] repeating units, and the five hydroximate oxygen atoms encapsulating a Bi^{3+} ion within the central cavity. Scalar relativistic DFT investigations predict similarity between molecular structures of the model bismuth(III) and lanthanum(III) tyrosinehydroximate 15-metallacrowns-5. At the same time analysis of the electronic structures reveals stronger donor-acceptor interactions between the central ion and the metallamacrocycle in the case of the lanthanum analogue. The larger density accumulation at the axial positions in the pentagonal pyramid ligand environment around the Bi^{3+} ion explains the preferential coordination of the negatively charged OH^- ion instead of the solvent molecule, as well as the exceptional six-coordinated geometry. Coordination of both Bi(III) and La(III) ions is characterized by significant π -contributions to the interactions with the metallamacrocycle. To conclude, we have prepared a new interesting bismuth(III) metallacrown complex, which may not only enrich the structure diversity of both metallacrowns and bismuth coordination compounds, but also offers another approach to discovery of new polynuclear metallamacrocyclic complexes with unconventional structures and properties.

Author Contributions: M.A.K., M.N.S., and S.Y.K. designed the research strategy; G.S.Z. synthesized compound **1**; R.V.R. performed X-ray analysis; G.Y.Z. performed DFT calculations; V.R.S. determined the thermochromic properties. All authors have read and agreed to the published version of the manuscript.

Funding: This research was funded by the Russian Foundation for Basic Research (RFBR Project 19-03-00755).

Acknowledgments: The study was carried out using the equipment of “Analytical Center of the IOMC RAS” with the financial support of the Federal objective program “Research and development in priority directions of advancement of science and technology complex of Russia for 2014-2020” (Unique project identifier is RFMEFI62120X0040).

Conflicts of Interest: The authors declare no conflict of interest.

References

1. Mjos, K.D.; Orvig, C. Metallodrugs in Medicinal Inorganic Chemistry. *Chem. Rev.* **2014**, *114*, 4540–4563. [[CrossRef](#)] [[PubMed](#)]
2. Gaynor, D.; Griffith, D. The prevalence of metal-based drugs as therapeutic or diagnostic agents: Beyond platinum. *Dalton Trans.* **2012**, *41*, 13239. [[CrossRef](#)] [[PubMed](#)]
3. Keogan, D.M.; Griffith, D. Current and Potential Applications of Bismuth-Based Drugs. *Molecules* **2014**, *19*, 15258–15297. [[CrossRef](#)] [[PubMed](#)]
4. Briand, G.G.; Burford, N. Bismuth Compounds and Preparations with Biological or Medicinal Relevance. *Chem. Rev.* **1999**, *99*, 2601–2658. [[CrossRef](#)] [[PubMed](#)]
5. Kowalik, M.; Masternak, J.; Barszcz, B.; Kowalik, J.M.A.B.B.M. Recent Research Trends on Bismuth Compounds in Cancer Chemoand Radiotherapy. *Curr. Med. Chem.* **2019**, *26*, 729–759. [[CrossRef](#)] [[PubMed](#)]
6. Sadler, P.J.; Li, H.; Sun, H. Coordination chemistry of metals in medicine: Target sites for bismuth. *Coord. Chem. Rev.* **1999**, *185*, 689–709. [[CrossRef](#)]
7. Yang, N.; Sun, H. Biocoordination chemistry of bismuth: Recent advances. *Coord. Chem. Rev.* **2007**, *251*, 2354–2366. [[CrossRef](#)]
8. Li, H.; Sun, H. Recent advances in bioinorganic chemistry of bismuth. *Curr. Opin. Chem. Biol.* **2012**, *16*, 74–83. [[CrossRef](#)]
9. Baranyai, Z.; Tirsoó, G.; Rösch, F. The Use of the Macrocyclic Chelator DOTA in Radiochemical Separations. *Eur. J. Inorg. Chem.* **2019**, *2020*, 36–56. [[CrossRef](#)]
10. Šimeček, J.; Hermann, P.; Seidl, C.; Bruchertseifer, F.; Morgenstern, A.; Wester, H.-J.; Notni, J. Efficient formation of inert Bi-213 chelates by tetraphosphorus acid analogues of DOTA: Towards improved alpha-therapeutics. *EJNMMI Res.* **2018**, *8*, 78. [[CrossRef](#)]
11. Stavila, V.; Davidovich, R.L.; Gulea, A.; Whitmire, K.H. Bismuth(III) complexes with aminopolycarboxylate and polyaminopolycarboxylate ligands: Chemistry and structure. *Coord. Chem. Rev.* **2006**, *250*, 2782–2810. [[CrossRef](#)]
12. Hakimi, M.; Motieyan, E.; Bertolotti, F.; Marabello, D.; Rodrigues, V.H. Three new bismuth(III) pyridine-2,6-dicarboxylate compounds: Synthesis, characterization and crystal structures. *J. Mol. Struct.* **2015**, *1099*, 523–533. [[CrossRef](#)]
13. Li, C.-H.; Jiang, J.-H.; Li, X.; Tao, L.-M.; Xiao, S.-X.; Gu, H.-W.; Zhang, H.; Jiang, C.; Xie, J.-Q.; Peng, M.-N.; et al. Synthesis, crystal structure and biological properties of a bismuth(III) Schiff-base complex. *RSC Adv.* **2015**, *5*, 94267–94275. [[CrossRef](#)]
14. Loh, A.; Ong, Y.C.; Blair, V.L.; Kedzierski, L.; Andrews, P.C. Bismuth(III) α -hydroxy carboxylates: Highly selective toxicity of glycolates towards *Leishmania major*. *J. Biol. Inorg. Chem.* **2015**, *20*, 1193–1203. [[CrossRef](#)] [[PubMed](#)]
15. Pathak, A.; Blair, V.L.; Ferrero, R.; Junk, P.C.; Tabor, R.; Andrews, P.C. Synthesis and structural characterisation of bismuth(III) hydroxamates and their activity against *Helicobacter pylori*. *Dalton Trans.* **2015**, *44*, 16903–16913. [[CrossRef](#)] [[PubMed](#)]
16. Pathak, A.; Blair, V.L.; Ferrero, R.L.; Mehring, M.; Andrews, P.C. Bismuth(III) benzohydroxamates: Powerful anti-bacterial activity against *Helicobacter pylori* and hydrolysis to a unique Bi 34 oxido-cluster [Bi 34 O 22 (BHA) 22 (H-BHA) 14 (DMSO) 6]. *Chem. Commun.* **2014**, *50*, 15232–15234. [[CrossRef](#)] [[PubMed](#)]
17. Keogan, D.M.; Twamley, B.; Fitzgerald-Hughes, D.; Griffith, D. Novel class of Bi(III) hydroxamato complexes: Synthesis, urease inhibitory activity and activity against *H. pylori*. *Dalton Trans.* **2016**, *45*, 11008–11014. [[CrossRef](#)]
18. Amiri, M.; Martin, N.P.; Sadeghi, O.; Nyman, M. Bismuth for Controlled Assembly/Disassembly of Transition-Metal Oxo Clusters, Defining Reaction Pathways in Inorganic Synthesis and Nature. *Inorg. Chem.* **2020**, *59*, 3471–3481. [[CrossRef](#)]

19. Mehring, M. From molecules to bismuth oxide-based materials: Potential homo- and heterometallic precursors and model compounds. *Coord. Chem. Rev.* **2007**, *251*, 974–1006. [[CrossRef](#)]
20. Yang, Y.; Ouyang, R.; Xu, L.; Guo, N.; Li, W.; Feng, K.; Ouyang, L.; Yang, Z.; Zhou, S.; Miao, Y. Review: Bismuth complexes: Synthesis and applications in biomedicine. *J. Coord. Chem.* **2015**, *68*, 379–397. [[CrossRef](#)]
21. Shannon, R.D. Revised effective ionic radii and systematic studies of interatomic distances in halides and chalcogenides. *Acta Crystallogr. Sect. A* **1976**, *32*, 751–767. [[CrossRef](#)]
22. Casely, I.J.; Ziller, J.W.; Mincher, B.J.; Evans, W.J. Bismuth Coordination Chemistry with Allyl, Alkoxide, Aryloxy, and Tetraphenylborate Ligands and the $\{[2,6-(\text{Me}_2\text{NCH}_2)_2\text{C}_6\text{H}_3]_2\text{Bi}\}^+\text{Cation}$. *Inorg. Chem.* **2011**, *50*, 1513–1520. [[CrossRef](#)] [[PubMed](#)]
23. Bodwin, J.J.; Cutland, A.D.; Malkani, R.G.; Pecoraro, V.L. The development of chiral metallacrowns into anion recognition agents and porous materials. *Coord. Chem. Rev.* **2001**, *216*, 489–512. [[CrossRef](#)]
24. Mezei, G.; Zaleski, C.M.; Pecoraro, V.L. Structural and Functional Evolution of Metallacrowns. *Chem. Rev.* **2007**, *107*, 4933–5003. [[CrossRef](#)] [[PubMed](#)]
25. Tegoni, M.; Remelli, M. Metallacrowns of copper(II) and aminohydroxamates: Thermodynamics of self assembly and host–guest equilibria. *Coord. Chem. Rev.* **2012**, *256*, 289–315. [[CrossRef](#)]
26. Happ, P.; Plenck, C.; Rentschler, E. 12-MC-4 metallacrowns as versatile tools for SMM research. *Coord. Chem. Rev.* **2015**, *289*, 238–260. [[CrossRef](#)]
27. Ostrowska, M.; Fritsky, I.O.; Gumienna-Kontacka, E.; Pavlishchuk, A.V. Metallacrown-based compounds: Applications in catalysis, luminescence, molecular magnetism, and adsorption. *Coord. Chem. Rev.* **2016**, *304–332*. [[CrossRef](#)]
28. Katkova, M.A. Water-Soluble Polynuclear Metallamacrocyclic Copper(II) and Lanthanide(III) Complexes Based on Amino Hydroxamic Acids. *Russ. J. Coord. Chem.* **2018**, *44*, 284–300. [[CrossRef](#)]
29. Zabrodina, G.S.; Katkova, M.A.; Baranov, E.V.; Zhigulin, G.Y.; Ketkov, S.Y. Synthesis and Molecular Structure of the First Metallamacrocyclic Bi(III)–Cu(II) 15-MC-5 Complex Derived from Pyrazinohydroxamic Acid. *Macroheterocycles* **2019**, *12*, 300–306. [[CrossRef](#)]
30. Katkova, M.A.; Zabrodina, G.S.; Muravyeva, M.S.; Shavyrin, A.; Baranov, E.V.; Khrapichev, A.A.; Ketkov, S.Y. Facile One-Pot Route toward Water-Soluble Lanthanide-Copper-Glycinehydroximate 15-Metallacrown-5 Complexes. *Eur. J. Inorg. Chem.* **2015**, *2015*, 5202–5208. [[CrossRef](#)]
31. Katkova, M.A.; Zabrodina, G.S.; Baranov, E.V.; Muravyeva, M.S.; Kluev, E.A.; Shavyrin, A.; Zhigulin, G.Y.; Ketkov, S.Y. New insights into water-soluble and water-coordinated copper 15-metallacrown-5 gadolinium complexes designed for high-field magnetic resonance imaging applications. *Appl. Organomet. Chem.* **2018**, *32*, e4389. [[CrossRef](#)]
32. Katkova, M.A.; Kremlev, K.V.; Zabrodina, G.S.; Rummyantsev, R.V.; Gazhulina, A.P.; Gusev, S.; Ketkov, S.Y.; Fomina, I.G.; Eremenko, I.L. Polynuclear Aminohydroximate Metallamacrocyclic Cu(II)–Ce(III) Complexes: A Facile Route to Intricate Nanostructures of Copper and Cerium Oxides. *Eur. J. Inorg. Chem.* **2019**, *2019*, 1002–1010. [[CrossRef](#)]
33. Katkova, M.A.; Zabrodina, G.S.; Rummyantsev, R.V.; Zhigulin, G.Y.; Ketkov, S.Y.; Lyssenko, K.A.; Fomina, I.G.; Eremenko, I.L. pH-Responsive Switching Properties of a Water-Soluble Metallamacrocyclic Phenylalaninehydroximate La(III)–Cu(II) Complex: Insight into Tuning Protonation Ligand States. *Eur. J. Inorg. Chem.* **2019**, *2019*, 4328–4335. [[CrossRef](#)]
34. Katkova, M.A.; Zabrodina, G.S.; Zhigulin, G.Y.; Rummyantsev, R.V.; Ketkov, S.Y. Water-Soluble Chiral Y(III)–Cu(II) Metallamacrocyclic Phenylalaninehydroximate Complex. *Russ. J. Coord. Chem.* **2019**, *45*, 721–727. [[CrossRef](#)]
35. Shayapov, V.R.; Usoltsev, A.N.; Adonin, S.A.; Sokolov, M.N.; Samsonenko, D.G.; Fedin, V.P.; Sokolov, M.N. Thermochromism of bromotellurates(IV): Experimental insights. *New J. Chem.* **2019**, *43*, 3927–3930. [[CrossRef](#)]
36. Turchenko, V.; Kalanda, N.; Yarmolich, M.; Balasoiu, M.; Lupu, N. Features of crystalline and magnetic structure of barium ferromolybdate in a wide temperature range. *J. Magn. Magn. Mater.* **2019**, *477*, 42–48. [[CrossRef](#)]
37. Cutland, A.D.; Malkani, R.G.; Kampf, J.W.; Pecoraro, V.L. Lanthanide [15]Metallacrown-5 Complexes Form Nitrate-Selective Chiral Cavities. *Angew. Chem. Int. Ed.* **2000**, *39*, 2689–2692. [[CrossRef](#)]
38. Battaglia, L.P.; Corradi, A.B.; Pelizzi, C.; Pelosi, G.; Tarasconi, P. Notes. Chemical and structural investigations on bismuth complexes of 2,6-di-acetylpyridine bis(2-thenoylhydrazone) and 2,6-diacetylpyridine bis(thiosemicarbazone). *J. Chem. Soc. Dalton Trans.* **1990**, 3857–3860. [[CrossRef](#)]

39. Yin, S.-F.; Maruyama, J.; Yamashita, T.; Shimada, S. Efficient Fixation of Carbon Dioxide by Hypervalent Organobismuth Oxide, Hydroxide, and Alkoxide. *Angew. Chem. Int. Ed.* **2008**, *47*, 6590–6593. [[CrossRef](#)]
40. Breunig, H.J.; Königsmann, L.; Lork, E.; Nema, M.; Philipp, N.; Silvestru, C.; Soran, A.; Varga, R.A.; Wagner, R. Hypervalent organobismuth(iii) carbonate, chalcogenides and halides with the pendant arm ligands 2-(Me₂NCH₂)C₆H₄ and 2,6-(Me₂NCH₂)₂C₆H₃. *Dalton Trans.* **2008**, *14*, 1831. [[CrossRef](#)]
41. Batsanov, S.S. Van der Waals Radii of Elements. *Inorg. Mater.* **2001**, *37*, 871–885. [[CrossRef](#)]
42. Katkova, M.A.; Zabrodina, G.S.; Zhigulin, G.Y.; Baranov, E.V.; Trigub, M.M.; Terentiev, A.A.; Ketkov, S.Y. The first water-soluble polynuclear metallamacrocyclic Sr(ii)–Cu(ii) complex based on simple glycinehydroximate ligands. *Dalton Trans.* **2019**, *48*, 10479–10487. [[CrossRef](#)] [[PubMed](#)]
43. Zhigulin, G.Y.; Zabrodina, G.S.; Katkova, M.A.; Ketkov, S.Y. DFT studies of the electron density distribution and donor-acceptor interactions in water-soluble aminohydroximate metallamacrocyclic CaII and YIII complexes. *Russ. Chem. Bull.* **2019**, *68*, 743–750. [[CrossRef](#)]
44. SAINT. *Data Reduction and Correction Program*; Bruker AXS: Madison, WI, USA, 2014.
45. Krause, L.; Herbst-Irmer, R.; Sheldrick, G.M.; Stalke, D. Comparison of silver and molybdenum microfocus X-ray sources for single-crystal structure determination. *J. Appl. Crystallogr.* **2015**, *48*, 3–10. [[CrossRef](#)]
46. Sheldrick, G.M. SHELXT—Integrated space-group and crystal-structure determination. *Acta Cryst.* **2015**, *A71*, 3–8. [[CrossRef](#)]
47. Sheldrick, G.M. Crystal structure refinement with SHELXL. *Acta Crystallogr. Sect. C Struct. Chem.* **2015**, *C71*, 3–8. [[CrossRef](#)]
48. Laikov, D.N. Fast evaluation of density functional exchange-correlation terms using the expansion of the electron density in auxiliary basis sets. *Chem. Phys. Lett.* **1997**, *281*, 151–156. [[CrossRef](#)]
49. Laikov, D.N.; Ustynyuk, Y.A. PRIRODA-04: A quantum-chemical program suite. New possibilities in the study of molecular systems with the application of parallel computing. *Russ. Chem. Bull.* **2005**, *54*, 820–826. [[CrossRef](#)]
50. Perdew, J.P.; Burke, K.; Ernzerhof, M. Generalized Gradient Approximation Made Simple. *Phys. Rev. Lett.* **1996**, *77*, 3865–3868. [[CrossRef](#)]
51. Laikov, D.N. A new class of atomic basis functions for accurate electronic structure calculations of molecules. *Chem. Phys. Lett.* **2005**, *416*, 116–120. [[CrossRef](#)]
52. Bader, R.F.W. *Atoms in Molecules: A Quantum Theory*; Oxford University Press: Oxford, UK, 1990.
53. Espinosa, E.; Molins, E.; Lecomte, C. Hydrogen bond strengths revealed by topological analyses of experimentally observed electron densities. *Chem. Phys. Lett.* **1998**, *285*, 170–173. [[CrossRef](#)]
54. Borissova, A.O.; Korlyukov, A.A.; Antipin, M.Y.; Lyssenko, K.A. Estimation of Dissociation Energy in Donor–Acceptor Complex AuCl–PPh₃ via Topological Analysis of the Experimental Electron Density Distribution Function. *J. Phys. Chem. A* **2008**, *112*, 11519–11522. [[CrossRef](#)] [[PubMed](#)]
55. Puntus, L.N.; Lyssenko, K.A.; Antipin, M.Y.; Bünzli, J.-C.G. Role of Inner- and Outer-Sphere Bonding in the Sensitization of EuIII-Luminescence Deciphered by Combined Analysis of Experimental Electron Density Distribution Function and Photophysical Data. *Inorg. Chem.* **2008**, *47*, 11095–11107. [[CrossRef](#)] [[PubMed](#)]
56. Abramov, Y.A. On the Possibility of Kinetic Energy Density Evaluation from the Experimental Electron-Density Distribution. *Acta Cryst.* **1997**, *53*, 264–272. [[CrossRef](#)]
57. Keith, T.A. *AIMAll*; Version 10.05.04; TK Gristmill Software: Overland Park, KS, USA, 2010.
58. Lu, T.; Chen, F. Multiwfn: A multifunctional wavefunction analyzer. *J. Comput. Chem.* **2011**, *33*, 580–592. [[CrossRef](#)]
59. Lu, T.; Chen, F. Quantitative analysis of molecular surface based on improved Marching Tetrahedra algorithm. *J. Mol. Graph. Model.* **2012**, *38*, 314–323. [[CrossRef](#)]
60. Frisch, M.J.; Trucks, G.W.; Schlegel, H.B.; Scuseria, G.E.; Robb, M.A.; Cheeseman, J.R.; Scalmani, G.; Barone, V.; Mennucci, B.; Petersson, G.A.; et al. *Gaussian 09*; Revision B.01; Gaussian Inc.: Wallingford, CT, USA, 2010.
61. Pollak, P.; Weigend, F. Segmented Contracted Error-Consistent Basis Sets of Double- and Triple- ζ Valence Quality for One- and Two-Component Relativistic All-Electron Calculations. *J. Chem. Theory Comput.* **2017**, *13*, 3696–3705. [[CrossRef](#)]

